AD-A086 665 HONEYWELL CORPORATE MATERIAL SCIENCES CENTER BLOOMIN--ETC F/G 20/6
OPTICAL INTERARRAY PROCESSING.(U)
MAR 80

UNCLASSIFIED

N0001&-80-C-0216

NL

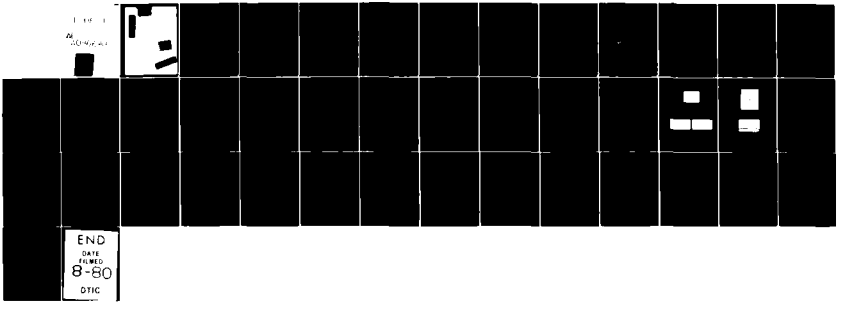

END
DATE FILMED
8-80
DTIC

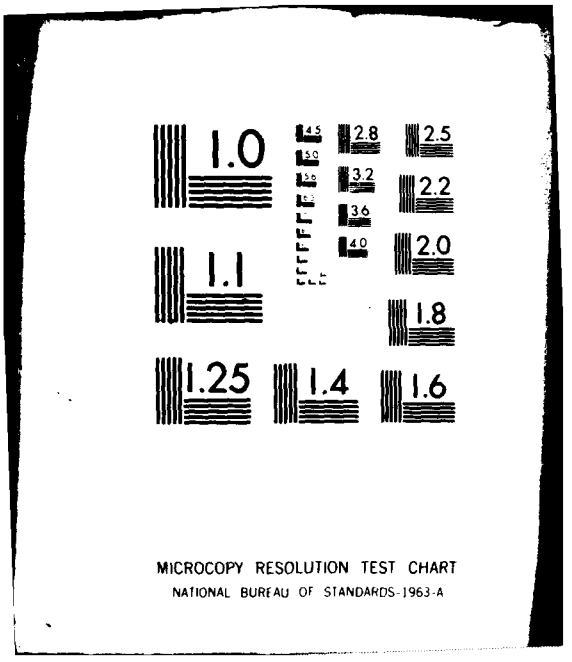
1.0
1.1
1.25
1.4
1.6
1.8
2.0
2.2
2.5
2.8
3.2
3.6
4.0
4.5
5.0
MICROCOPY RESOLUTION TEST CHART
NATIONAL BUREAU OF STANDARDS-1963-A

(12)

(9) Final Report. 1 Oct 79 - 31 [illegible].

to

Office of Naval Research

Contract No. N00014-80-C-0216

(15)

(6) OPTICAL INTERARRAY PROCESSING.

(11) Mar[redacted]80

(12) 41

DTIC

Honeywell [redacted].
Corporate Material Sciences Center,
10701 Lyndale Avenue South
Bloomington, Minnesota 55420



410 336

mt

TABLE OF CONTENTS


| Section | | Page |
|---|---|---|
| 1 | INTRODUCTION | 1 |
| 2 | OPTICAL DESIGN | 2 |
| | 2.1 Passive Optical Tau-Shift (POTS) Approach | 3 |
| | 2.2 Linear Phase Shifter (LIPS) Approach | 8 |
| 3 | NON-REAL TIME EXPERIMENTS | 16 |
| | 3.1 Experimental Results | 19 |
| | 3.2 Resolution and Accuracy | 22 |
| 4 | REAL TIME SYSTEM DESIGN | 24 |
| | 4.1 System Overview | 24 |
| | 4.2 Front End Electronics | 26 |
| | 4.2.1 TBC Buffer | 28 |
| | 4.2.2 RF Driver/Modulator | 32 |
| | 4.2.3 Data Preparation | 33 |
| | 4.3 Rear End Electronics | 33 |
| | 4.3.1 Two Dimensional Detector Array | 33 |
| | 4.3.2 Video Memory | 34 |
| 5 | SUMMARY | 35 |
| | REFERENCES | 37 |

## LIST OF ILLUSTRATIONS


| Figure | | Page |
|---|---|---|
| 1 | Geometrical relation of the two functions to be multiplied | 4 |
| 2 | Ambiguity function generation from one dimensional input transducers | 5 |
| 3 | POTS optical layout for ambiguity function generation using Bragg cells | 7 |
| 4 | LIPS optical layout for ambiguity function generation using Bragg cells | 10 |
| 5 | Construction of space variant linear phase shifter from conventional optics | 15 |
| 6 | POTS experimental layout | 17 |
| 7 | LIPS experimental layout | 18 |
| 8 | Ambiguity function of NOSC data produced by POTS | 20 |
| 9 | Scanning traces along the range axis (a) and the frequency axis (b) | 20 |
| 10 | Ambiguity function of V-FM signal produced by LIPS | 21 |
| 11 | Scanning trace along one ridge of the V-FM ambiguity function | 21 |
| 12 | Real time system overview | 25 |
| 13 | TBC buffer block diagram | 29 |


## LIST OF TABLES


| Table | | Page |
|---|---|---|
| 1 | System Design Specifications | 27 |

# SECTION 1
# INTRODUCTION

This final report covers work performed during the period from October 1, 1979 to March 31, 1980 under ONR Contract No. N00014-80-C-0216 on the subject "Optical Interarray Processing".

The objectives of this contract were to design and demonstrate an optical architecture capable of non-real time generation of ambiguity functions from one dimensional input transducers, and design the front end and rear end electronics necessary to support real time operation of such a processor. In the following sections we will describe the work we have performed to achieve these objectives. The actual construction of the front end and rear end electronics is not part of this contract. However, it will be part of the newly awarded ONR Contract No. N00014-80-C-0429.

## SECTION 2
## OPTICAL DESIGN

The ambiguity function $\chi(\nu,\tau)$ for two given signals $f_2(t)$ and $f_2(t)$ is defined by

$$\chi(\nu,\tau) = \int_{-\infty}^{\infty} f_1(t)\, f_2^*(t-\tau)\, e^{-j2\pi\nu t} dt. \qquad (1)$$

In the past (1-5), the spatial integration methods used for optically computing the ambiguity function have all required two dimensional input transducers. This requirement effectively placed a ceiling on the throughput of the optical processor in that it could not exceed the frame rate of the two dimensional input transducer that was chosen. Currently available two dimensional input transducers have maximum frame rates of around 30 frames/sec.

One dimensional input transducers such as acousto-optic Bragg cells have much higher frame rates. For example, a $TeO_2$ Bragg cell 30 mm in length has a frame time of only 48 μsec. Bragg cells also offer the advantages of electronic data composing and high diffraction efficiency.

We have invented a spatial integration approach called Passive Optical Tau-Shift (POTS) that uses one dimensional input transducers. We have also invented another spatial integration approach which uses a space variant Linear Phase Shifter (LIPS) and also accepts one dimensional input transducers. Both approaches will be described in the following paragraphs.

## 2.1 PASSIVE OPTICAL TAU-SHIFT (POTS) APPROACH

If we look at equation (1), it is clear that the product of the signals $f_1(t)$ and $f_2^*(t-\tau)$ will reside in a two dimensional plane $(t,\tau)$. However, each signal itself is a function of t only and hence one dimensional in nature. The representation of $f_1(t)$ in a $(t,\tau)$ plane (Figure 1) can be thought of as the one dimensional signal $f_1(t)$ stretched vertically along the $\tau$ axis. Similarily, the representation of $f_2(t-\tau)$ in a $(t,\tau)$ plane can be thought of as the one dimensional signal $f_2(t)$ stretched along the line $t-\tau$, making some angle $\theta$ with the $\tau$ axis.

Stretching one dimensional signals can be accomplished easily by cylindrical lenses. An implementation of this idea for producing the ambiguity function is shown in Figure 2, where Bragg cells are assumed as input transducers.

The one dimensional signal $f_2^*(x')$ in Bragg cell I is diverged along the y' axis by a cylindrical lens placed along the x' axis, where the x'-y' coordinate system is tilted with respect to the x-y coordinate system by some angle $\theta$. The stretched version of $f_2(x')$ is then demagnified to preserve the proper scale with respect to the x-y coordinate system, and converged along the y axis to form a line on Bragg cell II in a geometrical sense. The field immediately after Bragg cell II will be the product function $f_1(x)f_2^*(x-\tau)$. By Fourier transforming this field with respect to x and imaging the intermediate plane in y, the desired ambiguity function of equation (1) will be produced.

The focal lengths of the cylindrical lenses $L_3$ and $L_4$ are chosen to be identical, while the focal lengths $f_2$ and $f_5$ of the spherical

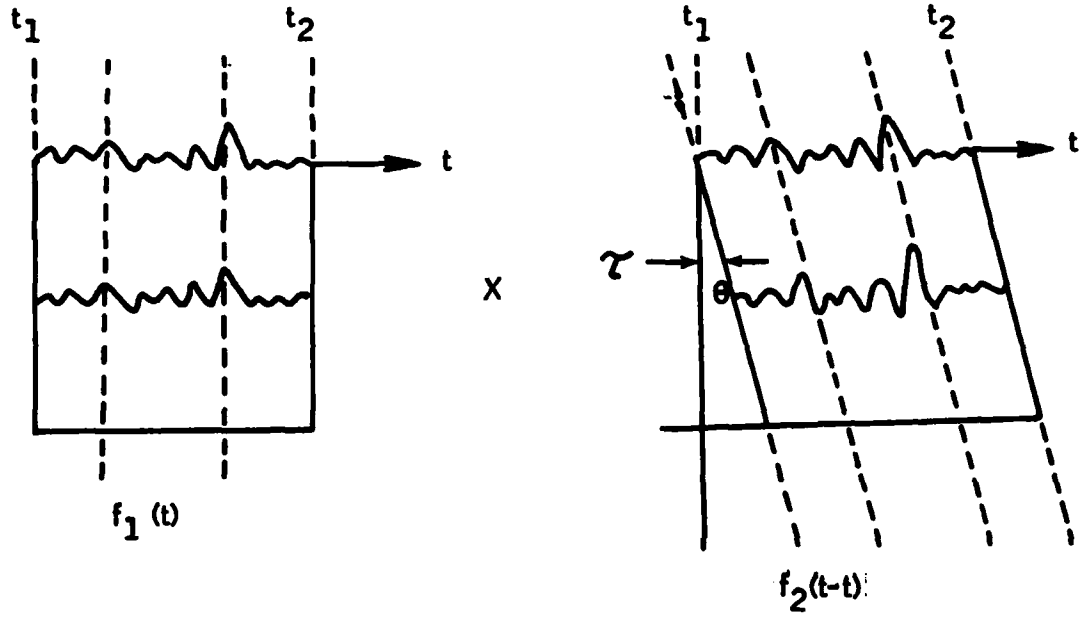


Figure 1. Geometrical relation of the two functions to be multiplied.

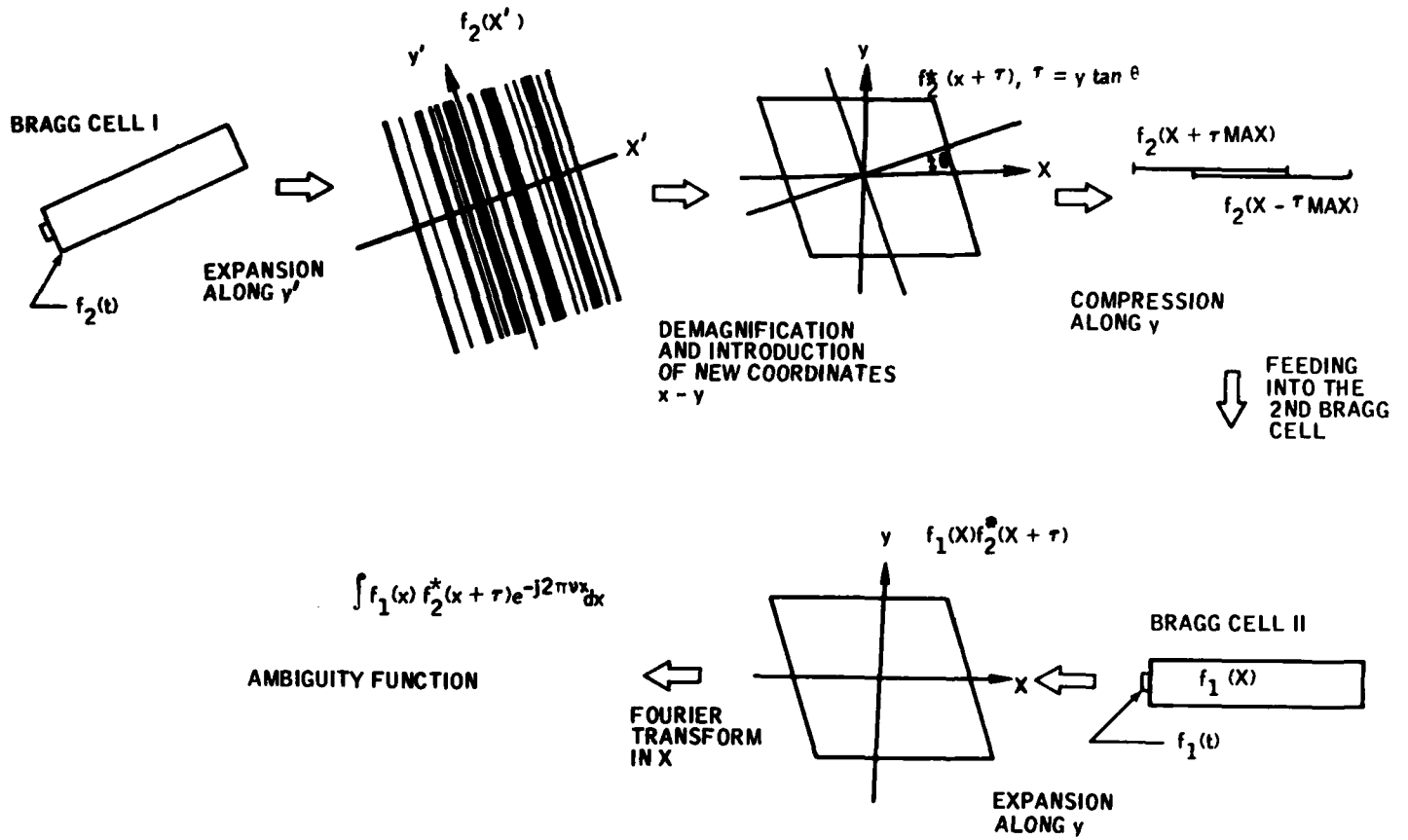


Figure 2. Ambiguity function generation from one dimensional input transducers.

lenses $L_2$ and $L_5$ are chosen such that their ratio is the demagnification factor, cos (θ), or

$$\frac{f_5}{f_2} = \cos(\theta). \tag{2}$$

A Bragg cell has a finite window height in the vertical (or transverse) dimension, and this imposes a limitation on the processor bandwidth and τ-shift. Bragg cell I receives a converging wavefront from cylindrical lens $L_1$ whose line width is negligible. The wavefront converging on Bragg cell II will have a spread in y due to the tilt of Bragg cell I with respect to the x-y coordinate system. The signal at plane A in Figure 3 will have a bandwidth $BW_A$ along the x' axis, and the spread Δy at Bragg cell II is due to the y component of $BW_A$, or

$$\Delta y = \lambda f_5 \, BW_A \sin(\theta) \tag{3}$$

where λ is the wavelength being used. Also, $BW_A$ is related to the bandwidth of the signal in the Bragg cell (BW) by

$$BW_A = \frac{f_2}{f_3} BW. \tag{4}$$

Combining (2), (3) and (4), we obtain

$$\Delta y = \frac{\lambda}{2} \frac{f_2^2}{f_3} BW \sin(2\theta). \tag{5}$$

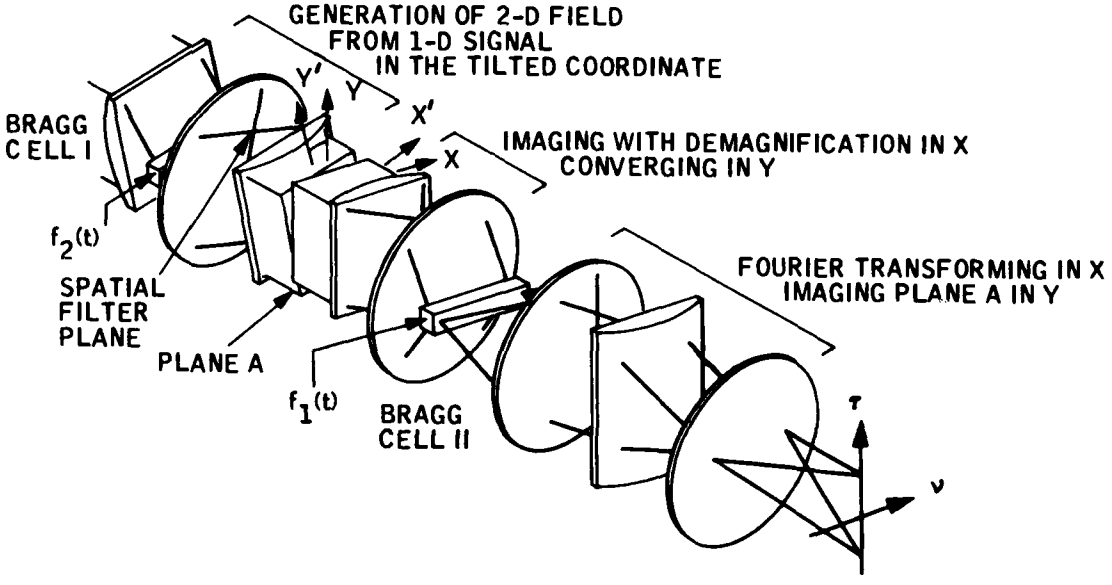


Figure 3. POTS optical layout for ambiguity function generation using Bragg cells.

It is easily seen from Figure 2 that the maximum τ-shift ($\tau_{max}$) is proportional to the time window, T, of the signal and the tangent of the tilting angle θ.

$$\tau_{max} = T \tan(\theta). \tag{6}$$

Since $\tan\theta \cong 1/2 \sin(2\theta)$ for small θ, we get

$$\Delta y \cong \lambda \frac{f_2^2}{f_3} BW \frac{\tau_{max}}{T}. \tag{7}$$

The spread in y at Bragg cell II is, therefore, proportional to the maximum τ-shift of the processor and the signal bandwidth in Bragg cell I, and a tradeoff will exist between the two quantities whenever Δy is larger than the effective window height of the one dimensional input transducer chosen.

We will use an acousto-optic modulator as a shutter to define the exposure time, which must be shorter than the time window of the Bragg cell. The acoustic signals in the two Bragg cells are imaged upon each other and travel with the same acoustic velocity so there is no misregistration during the exposure time.

## 2.2 LINEAR PHASE SHIFTER (LIPS) APPROACH

In the previous paragraph we showed how the POTS approach can create the two dimensional field $f_2(t-\tau)$ from one dimensional input transducers. This is done essentially by coordinate rotation followed by demagnification. In the LIPS approach we generate the τ-shift by shear instead of rotation.

This shear concept is depicted in Figure 4. The telecentric spherical lens pair $S_3$ And $S_4$ forms the image of Bragg cell I and $f_2(t)$ onto Bragg cell II and $f_1(t)$ through a linear phase shifter in the Fourier plane. The presence of the linear phase shifter causes a position shift of the image, and this misregistration accomplishes the $\tau$-shift. By spatially varying the slope of the linear phase shifter along the vertical direction, the system spatially scans continuously in the $\tau$ axis. Lens $S_5$ performs a spatial integration to yield the desired ambiguity function. We will now analyze this system in formal Fourier mathematics to prove that this concept is sound.

The Bragg cells accept temporal signals $f_2(t)$ and $f_1(t)$ and convert them into a running transmissivity function $f_2(t - \frac{x}{v})$. At an instant in time we can consider them as the spatial transmissivity function B1 and B2 with an appropriate scaling factor.

$$B1 = f_2(x) \tag{8}$$

$$B2 = f_1(x) \tag{9}$$

A linear phase shifter is placed in the Fourier plane to shift the phase according to $\phi = 2\pi\xi\eta$ (see Figure 4) where $\xi$ and $\eta$ are the coordinates in the Fourier plane. Thus the transmissivity function of this linear phase shifter (LPS) is

$$LPS = e^{j2\pi\xi\eta}. \tag{10}$$

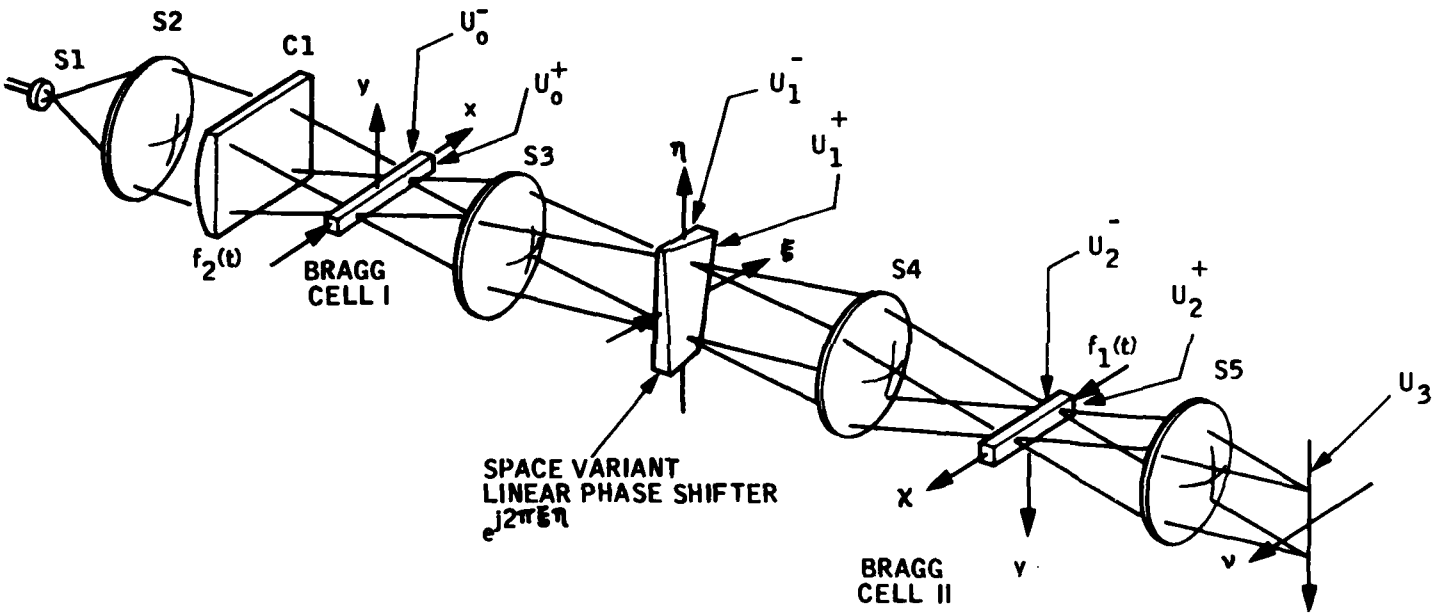


Figure 4. LIPS optical layout for ambiguity function generation using Bragg cells.

The process of this cascade optical system can be explained effectively using mathematical manipulations to show how this system generates the ambiguity function in the final plane. The optical fields are notated by $U_o$, $U_1$, ... corresponding to plane 0, plane 1, .... The superscript - and + indicate the field immediately before and after the device.

First, $U_o^-$ can be approximated by a horizontal line,

$$U_o^- = \delta(y). \tag{11}$$

The first Bragg cell modulates this line into

$$U_o^+ = f_2(x)\, U_o^- = f_2(x)\, \delta(y). \tag{12}$$

Lens $S_3$ takes the Fourier transform of this field to give

$$U_1^- = \int\int U_o^+ \, e^{-j2\pi(\xi x+\eta y)} \, dx \, dy = F_2(\xi). \tag{13}$$

This goes through the linear phase shifter to become

$$U_1^+ = e^{j2\pi\xi\eta} \, U_1^- = F_2(\xi) \, e^{j2\pi\xi\eta} \tag{14}$$

Lens $S_4$ takes the Fourier transform to give

$$U_2^- = \iint U_1^+ \, e^{-j2\pi(\xi x + \eta y)} \, d\xi \, d\eta$$

$$= \int F_2(\xi) \left[ \int e^{j2\pi\xi\eta} \, e^{-j2\pi\eta y} \, d\eta \right] e^{-j2\pi\xi x} \, d\xi$$

$$= \int F_2(\xi) \, \delta(\xi - y) \, e^{-j2\pi\xi x} \, d\xi.$$

$$U_2^- = F_2(y) \, e^{-j2\pi xy}. \qquad (15)$$

Equation (15) indicates that the height of the pattern is the bandwidth of the signal $f_1(x)$. If the height of the Bragg cell's effective window is larger than the bandwidth, there is no loss of information due to the narrowness of the Bragg cell window.

$$U_2^+ = f_1(x) \, U_2^- = f_1(x) \, F_2(y) \, e^{-j2\pi xy}. \qquad (16)$$

Lens $S_5$ takes the Fourier transform of this field and displays it in the plane 3

$$U_3 = \iint U_2^+ \, e^{-j2\pi(\xi x - \eta y)} \, dx \, dy.$$

$$= \int f_1(x) \left[ \int F_2(y) \, e^{-j2\pi xy} \, e^{j2\pi\eta y} \, dy \right] e^{-j2\pi\xi x} \, dx.$$

$$U_3 = \int f_1(x) \, f_2(x - \eta) \, e^{-j2\pi\xi x} \, dx. \qquad (17)$$

Equation (17) clearly shows that the ambiguity function defined by equation (1) is achieved in the spatial frequency space $(\xi, \eta)$. The conjugation of signal $f_2(x)$ can be obtained by putting the signal on a carrier and evaluating the first diffraction order

with the aid of a vertical slit in plane 1. The mathematics manipulated in equation (8) through equation (17) are essentially the same to achieve

$$U_3 = \int f_1(x)\, f_2^*(x-\eta)\, e^{-j2\pi\xi x}\, dx. \tag{18}$$

It is clear that equation (18) is a spatial representation of the desired ambiguity function, and we can obtain equation (1) by converting the spatial variables into the temporal variables with the appropriate conversion factors.

The feasibility of implementing the LIPS approach depends heavily on the manufacturability of the linear phase shifter element. It is essentially an optical wedge whose wedge angle linearly changes with height. The complex transmissivity function of this components in rectangular coordinates is given by

$$g(x,y) = e^{j\alpha xy} \tag{19}$$

where $\alpha$ is a constant.

Conventional manufacturing processes such as grinding and polishing a glass piece would be difficult if not impossible to apply to the fabrication of such an element. We have invented a method to fabricate this component out of conventional optics, hence high accuracy of the transmitted wavefront is possible.

By modifying equation (19), we have

$$g(x,y) = e^{j\frac{\alpha}{2}(x+y)^2}\, e^{-j\frac{\alpha}{2}(x^2+y^2)}. \tag{20}$$

Define $r = x^2 + y^2$ and introduce a coordinate system (x',y') that is rotated from (x,y) by $45^o$ (Figure 5). Then equation (20) can be rewritten as

$$g(x,y) = e^{j\alpha x'^2} \; e^{-j\frac{\alpha}{2} r^2} . \qquad (21)$$

The first exponent in equation (21) is the complex transmissivity function of a cylindrical lens oriented parallel to the x' axis. The second exponent is a spherical lens. The cylindrical lens is twice as powerful as the spherical lens, and the sign is opposite.

Therefore, the space variant linear phase shifter can be accurately fabricated by cementing a cylindrical lens and a spherical lens of opposite power together, and orienting them at $45^o$. The focal length of the cylindrical lens should be half that of the spherical lens.

The LIPS approach has the advantages of fewer cylindrical lenses, fewer optical components, and much shorter optical path length. Experimental evaluations of both systems will be reported in the next section.

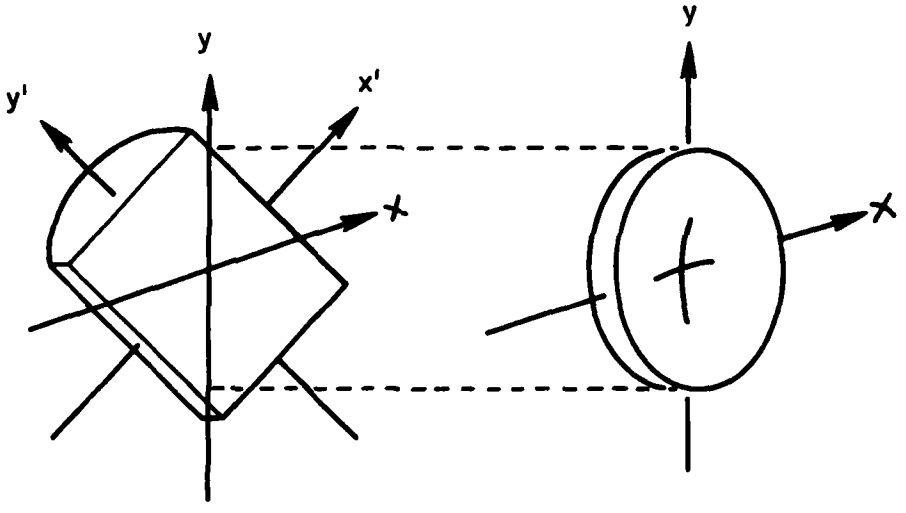


Figure 5. Construction of space varient linear phase shifter from conventional optics.

## SECTION 3
## NON-REAL TIME EXPERIMENTS

To test the validity of the POTS and LIPS architectures, both systems were constructed, and experiments carried out in a non-real time mode using photographic transparencies as input transducers. The focal lengths of the lenses for both test systems were deliberately chosen to be very long so that the necessary optical components could be quickly and easily obtained and aberrations in the systems could be kept to a minimum.

For example, the cylindrical lenses in the POTS archiecture had 800 mm focal lengths, giving the system an f number of f/30, and a total system length of 12 meters. The cylindrical lens $C_1$ in the LIPS architecture was also 800 mm in focal length, and the telecentric imaging lenses were 762 mm in focal length. The linear phase shifter element was constructed from a 250 mm single element cylindrical lens, and a 505 mm single element negative spherical lens. Both lenses were off-the-shelf components. Even with such long focal lengths, the total system length for LIPS was 5.5 meters, considerably shorter than the 12 meters for POTS, although the two systems had nearly the same f number. The focal lengths of all the lenses for both systems are shown in Figures 6 and 7.

The photographic transparencies used in evaluating the two systems were created using a computer-driven precision CRT plotter and high resolution microfilm. Since the synthetic data on the NOSC tape is complex, it must be placed on a carrier frequency to preserve the phase information of the original signal. The NOSC data is, therefore, plotted according to the formula

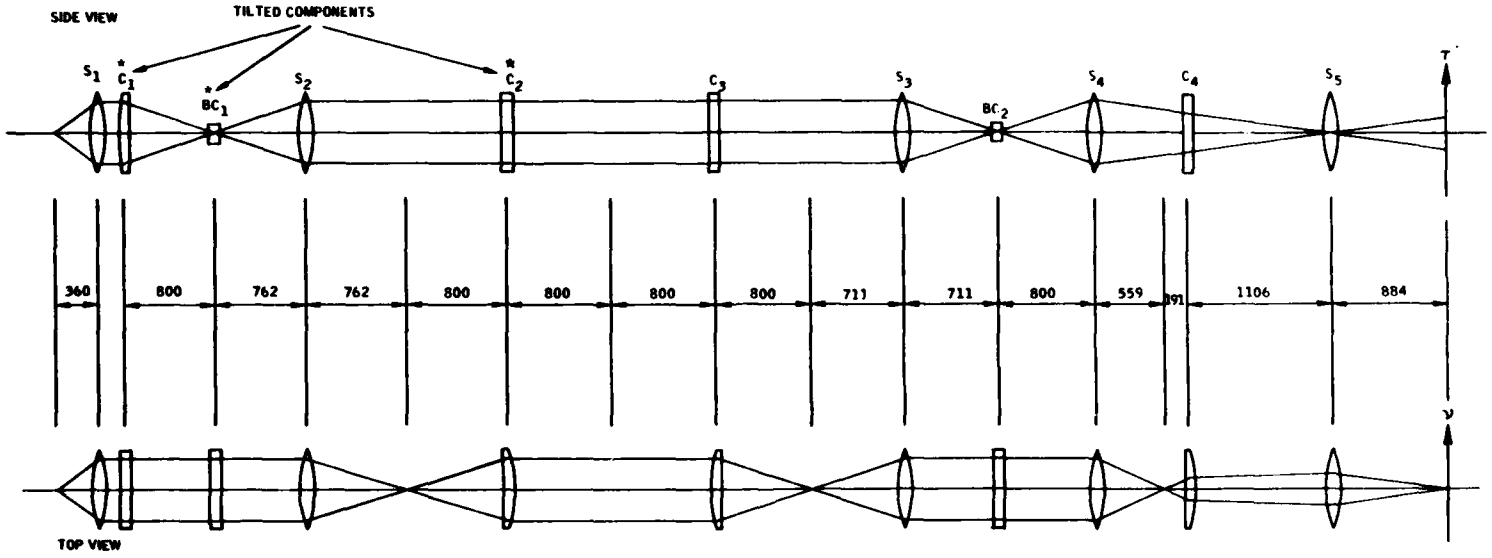


SPHERICAL LENSES

| LENS | FOCAL LENGTH (MM) |
|---|---|
| $S_1$ | 360 |
| $S_2$ | 762 |
| $S_3$ | 711 |
| $S_4$ | 559 |
| $S_5$ | 762 |

CYLINDRICAL LENSES

| LENS | FOCAL LENGTH (MM) |
|---|---|
| $C_1$ | 800 |
| $C_2$ | 800 |
| $C_3$ | 800 |
| $C_4$ | 200 |

Figure 6. POTS experimental layout.

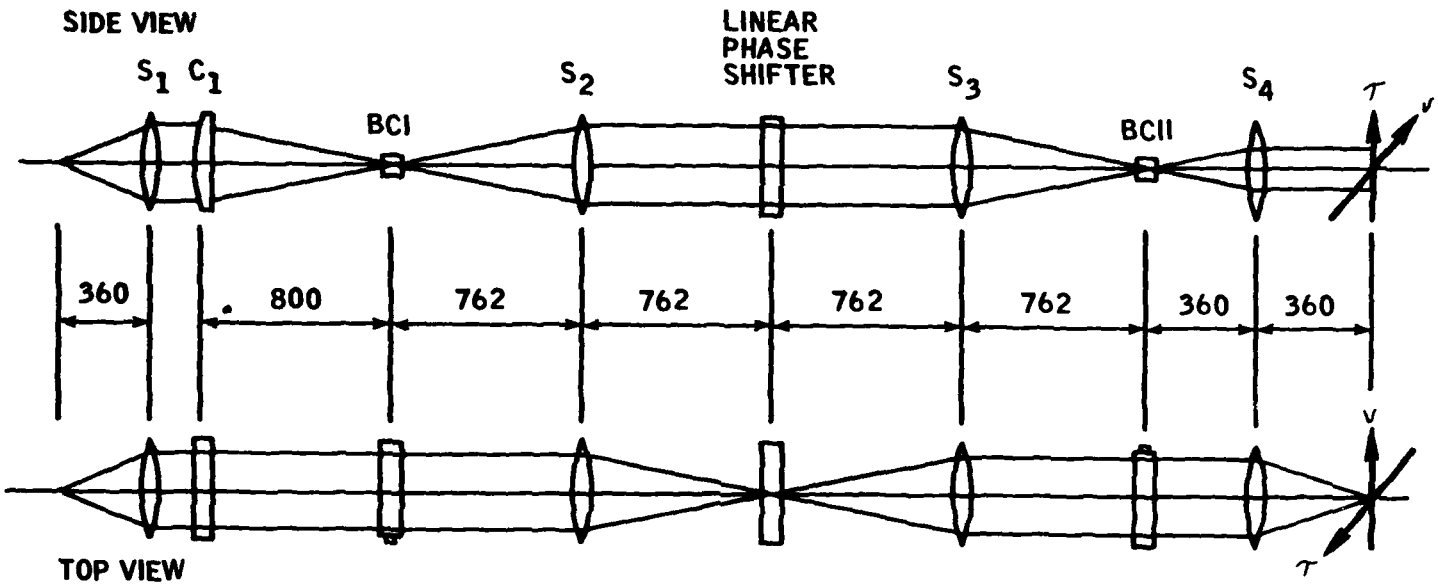


SPHERICAL LENSES

| LENS | FOCAL LENGTH (MM) |
|---|---|
| $S_1$ | 360 |
| $S_2$ | 762 |
| $S_3$ | 762 |
| $S_4$ | 360 |

CYLINDRICAL LENSES

| LENS | FOCAL LENGTH (MM) |
|---|---|
| $C_1$ | 800 |

Figure 7. LIPS experimental layout.

$$R(t)\cos(2\pi\nu_c t) - I(t)\sin(2\pi\nu_c t) + B. \quad (22)$$

where R(t) and I(t) are the real and imaginary values of the signal at time t, $\nu_c$ is the chosen carrier frequency, and B is a bias value chosen such that only positive values will be generated for plotting.

The physical size of a plotted transparency was chosen to simulate a Bragg cell, so it measures 24 mm long by 3 mm high. When used in the experimental optical processors the transparencies were placed in liquid gates filled with index-matching fluid.

## 3.1 EXPERIMENTAL RESULTS

An example of an ambiguity function generated by the POTS architecture is shown in Figure 8. In this case, the input signal-to-noise ratio (SNR) was 0 dB. Scanning traces along the range and doppler axes are shown in Figure 9 and they show a good output SNR with the peak clearly standing out from the surrounding noise.

An example of an ambiguity function generated by the LIPS architecture is shown in Figure 10. In this case, the input signal was a V-FM signal composed of two symmetric wings of linear chirp of the form $e^{i\alpha t^2}$ joined at the middle. This is a very useful test signal since its ambiguity function is well-known.[6,7] The ratio of the central peak height to the shoulder height immediately adjacent to the peak should be 4 to 1, and this is confirmed by the scanning trace in Figure 11.

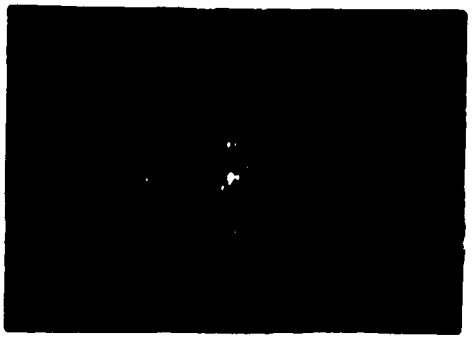

Figure 8. Ambiguity function of NOSC data produced by POTS.

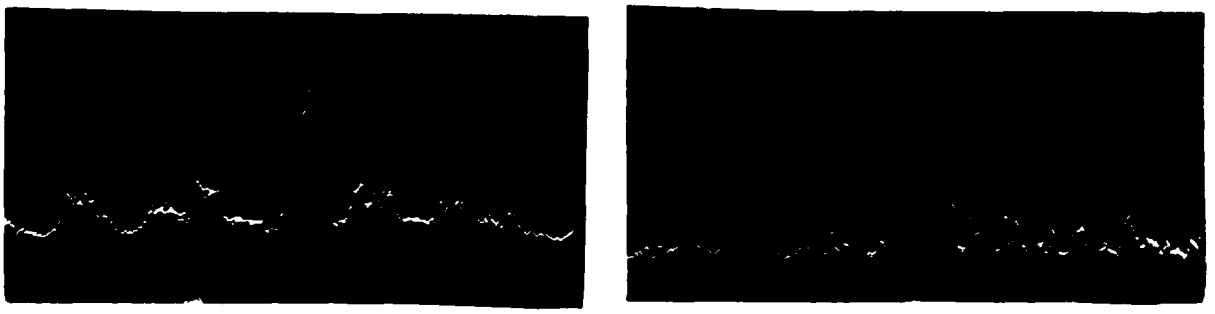

(b)

Figure 9. Scanning traces along the range axis (a) and the frequency axis (b).

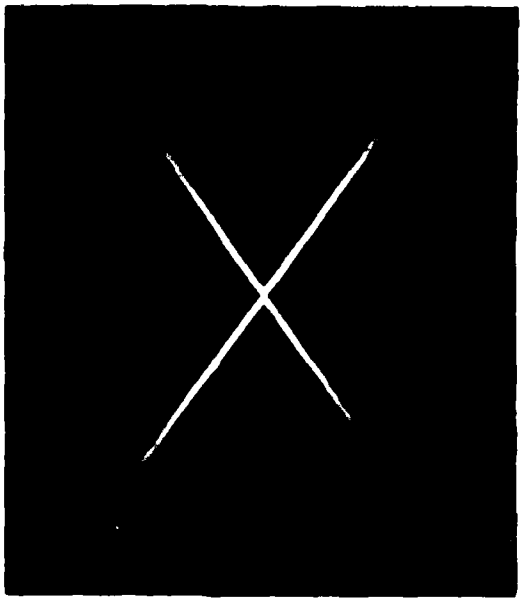

Figure 10. Ambiguity function of V-FM signal produced by LIPS.

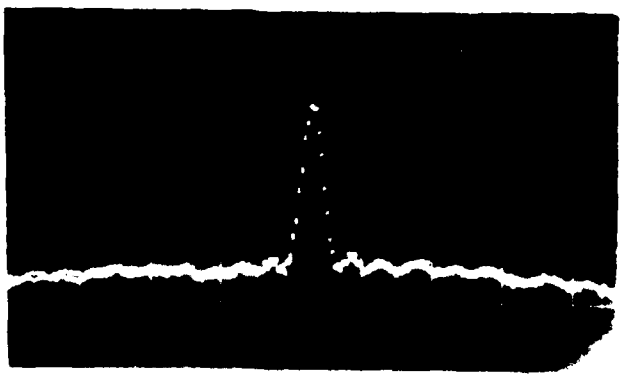

Figure 11. Scanning trace along one ridge of the V-FM ambiguity function.

## 3.2 RESOLUTION AND ACCURACY

The resolution of an ambiguity function is related to the signal bandwidth (BW) and the length of the time window (T) by the well-known relations

$$\Delta\nu = \frac{1}{T} \qquad \Delta\tau = \frac{1}{BW} \tag{23}$$

The scanning traces in Figure 9 were taken from an ambiguity function whose input signals had signal bandwidths of 0.1 Hz and time windows of 600 seconds. Both traces were calibrated for scale, and their resolutions at the half power points of the central peaks were determined. For the frequency axis, the resolution was found to be 1.59 mHz, compared to 1.68 mHz predicted by theory. For the range axis, the resolution was found to be 9.7 seconds, compared to a theoretical prediction of 10 seconds. Both resolutions are therefore in excellent agreement with the relations in equation (23), a result which was typical of all the optically produced ambiguity functions.

To check the accuracy of an optically produced ambiguity function, either the ambiguity integral for two given signals must be calculated digitally, or a signal whose ambiguity function structure is well-known can be chosen and processed optically, and the results compared. The V-FM signal falls into the latter category. The ambiguity function of the V-FM signal produced by the LIPS architecture was previously noted to be in good agreement with the calculated ambiguity function in its peak height to shoulder height ratio.

Also present in the optically processed ambiguity function is excellent symmetry about the range and doppler axes, and a fine structure of ripples running between the diagonal arms of the ambiguity function, as clearly present in both the photograph and the scanning trace. The symmetrical presence of this structural detail, which is predicted by calculation, indicates that a very accurate ambiguity function has been produced. V-FM ambiguity functions having such excellent detail were produced by both the POTS and LIPS architectures.

The two optical processing architectures investigated have the common advantage of using one dimensional Bragg cells as input transducers, and both can produce accurate ambiguity functions. The LIPS architecture also has the additional advantages of being inherently much shorter in optical path length, and it requires fewer optical components. Finally, the LIPS architecture requires only one cylindrical lens of quality, while the POTS architecture requires at least three. It is clear that the LIPS architecture has more potential to become a relatively small, compact, optical processor.

# SECTION 4
# REAL TIME SYSTEM DESIGN

In the previous section we showed that our optical system can generate the two dimensional ambiguity function using one dimensional nonreal time input transducers. This section will discuss the system we have designed to realize real time operation of the optical processor. The one dimensional input transducers that were simulated by transparencies will be replaced by acousto-optic Bragg cells which can accept real time electronic signals and convert them from the time domain to the space domain. The output of the optical processor will be detected by a two dimensional photodiode array and converted into an electrical signal for output from the system.

## 4.1 SYSTEM OVERVIEW

The real time system is designed around the optical ambiguity function generator utilizing two Bragg cells (Figure 12). The front end electronics, consisting of a time base compression (TBC) buffer, two digital-to-analog converters (DACs), and two RF driver/modulators, receives the input signals from the HP 9825A calculator in digital form and converts them to analog signals which cause index of refraction modulations in the Bragg cells which are proportional to the input signals. The rear end electronics, consisting of a two dimensional detector array camera and a video memory, captures the ambiguity function, displays it on a CRT, and digitizes and stores it for examination.

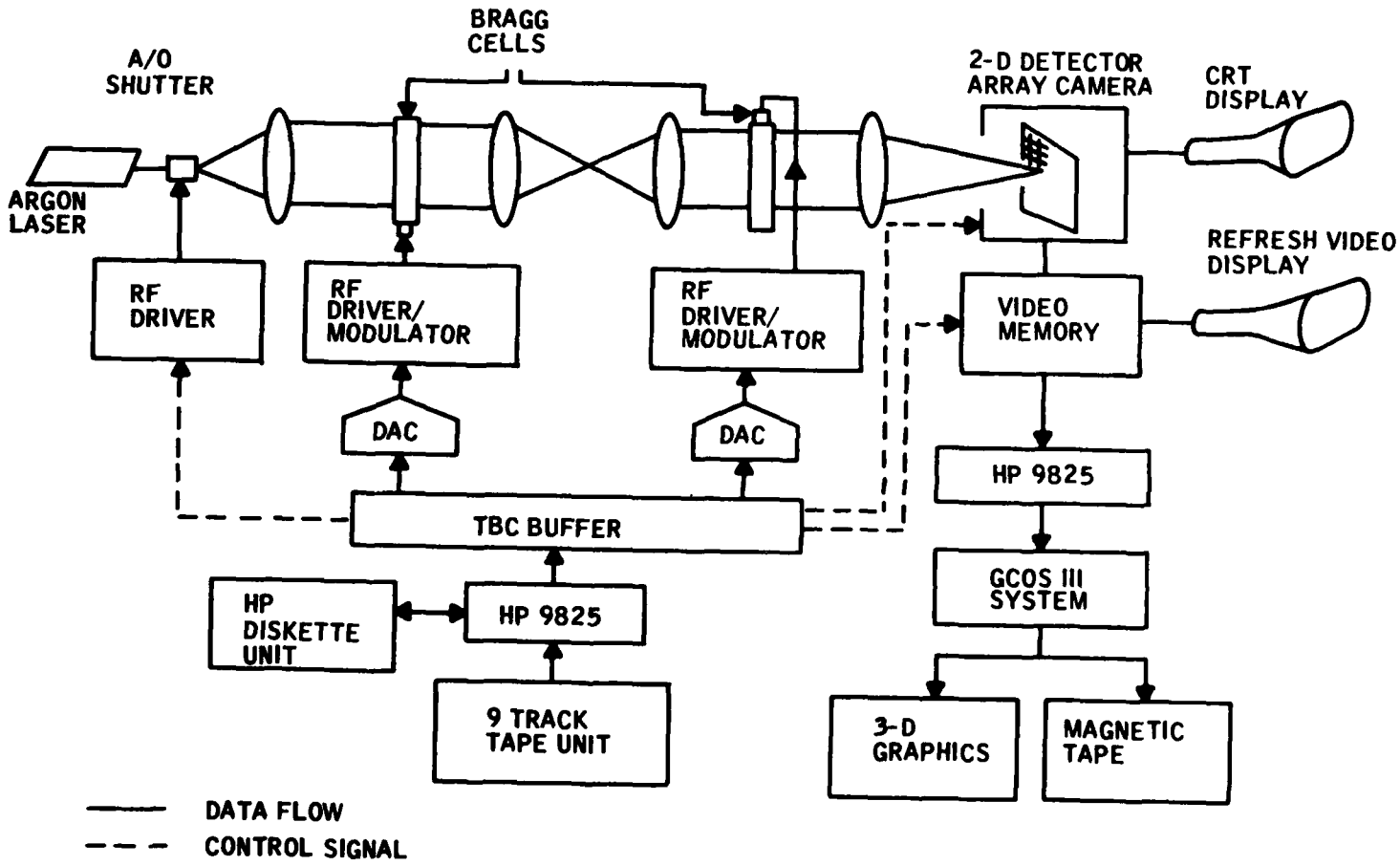


Figure 12. Real time system overview.

The optical source is a one watt Argon laser, and an acousto-optic modulator acts as a shutter. Shutter operation, camera activation, and data transfer into the video memory are all controlled by timing control signals from the TBC buffer.

The system design specifications are listed in Table 1. The design processing speed of the real time system is 500 frames/sec and the system time-bandwidth product is 240. This real time system is interfaced to an HP 9825A calculator for system performance evaluation purposes. Details of the subsystems are discussed in the following paragraphs.

## 4.2 FRONT END ELECTRONICS

The most important design criterion in the front end electronics is the system time-bandwidth product (TBW). An acoustic shear wave in a $TeO_2$ Bragg cell will propagate with a speed of 617 meters/sec, while the practical physical window size is 30 mm. Therefore, it takes only 48 μsec for the acoustic wave to propagate through the window. A sufficient system TBW therefore requires a fast data rate and high speed DACs. The fastest 8 bit DAC commercially available operates at a 50 MHz data rate, and a digital TBC buffer of comparable speed must be constructed to operate with it. The following paragraphs describe the TBC buffer design based on a concept of multiplexing emitter-coupled-logic (ECL) memories. Also described will be the RF driver-modulators and data preparation.

Table 1. System Design Specifications

| | |
|---|---|
| **Bragg Cells** | |
| Physical Length | 30 mm |
| Time Window | 48 μsec |
| **Time Base Compression Buffer** | |
| Size | 1920 bytes x 2 channels |
| Data Rate | 50 Mbytes/sec |
| Maximum Signal Time Window | 38.4 μsec |
| **Data Preprocessing** | |
| Bandwidth | 0.25 Hz |
| Subcarrier | 0.4 Hz |
| Sampling Rate | 5 points/carrier cycle |
| **RF Driver** | |
| Driver No. 1 | Center frequency 45 MHz |
| Driver No. 2 | Center frequency 75 MHz |
| **System Processing Rate** | 500 Frames/sec |
| **System Time-Bandwidth Product** | 240 |

### 4.2.1 TBC Buffer

This buffer is an electronic system designed to provide the required time base compression between very slow data storage devices such as magnetic tape, disk, or digital memory, and very fast optical devices such as Bragg cells. The component design used for this task is ECL circuitry which can provide the speed capability needed in this buffer. The TBC buffer is designed to accept a 16 bit parallel direct-memory-access (DMA) word with handshake and control lines from a HP 9825A calculator through a HP 98032A interface connection.

The TBC buffer has the following nine basic circuit blocks (see Figure 13):

1. I/O Translators
2. Clock
3. Controller
4. Address Generator
5. Memory
6. Parity and Display
7. Demultiplex
8. Line Driver
9. Digital-to-Analog Converter (DAC).

Circuit blocks 1 through 8 are contained on one Augat 3 layer, 5 level, wire-wrap circuit board which provides low noise, high frequency, high density, and accurate system performance.

1. I/O Translators -- Translator circuits are used at all I/O ports to convert from TTL logic to ECL logic, and vice versa. These ports include command byte, data word, peripheral signals, handshake, and control line activity.

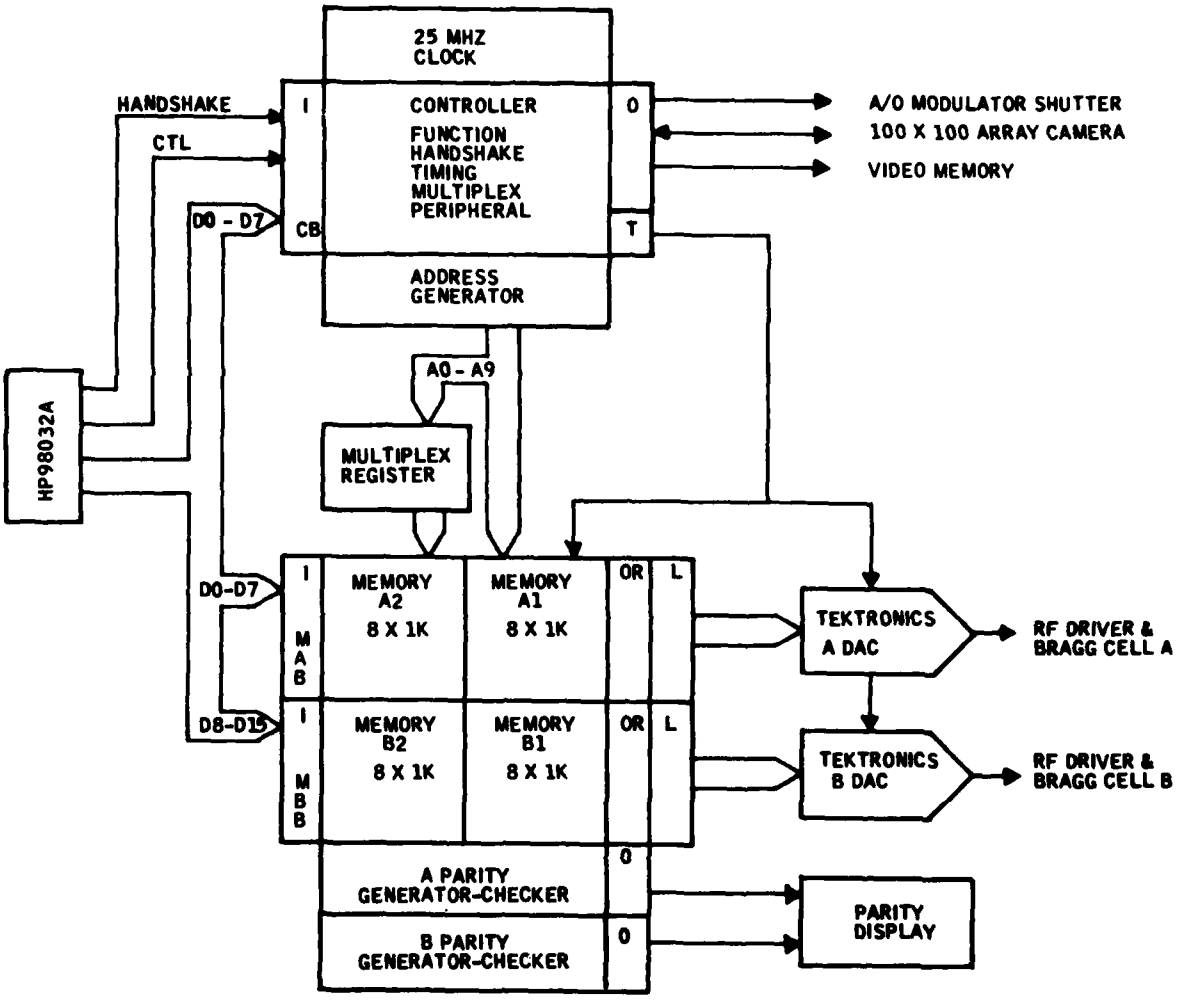


I INPUT TRANSLATORS
O OUTPUT TRANSLATORS
CB CONTROL BYTE
MAB MEMORY A BYTE
MBB MEMORY B BYTE
OR OR'S A1 AND A2
L LINE DRIVERS
T TIMING

Figure 13. TBC buffer block diagram.

2. Clock -- A 25 MHz frequency generator is used to clock and synchronize the TBC buffer. This generator is an RC-coupled voltage controlled multivibrator. The clock signal is divided by two to provide the two phases required for multiplexing.

3. Controller -- The internal operation of the TBC buffer and the response of the peripherals connected to it are determined by the controller circuits which operate under program control and perform the following tasks:

a. Function -- The command instruction from the HP calculator that selects the peripheral configuration, e.g., write memory, read memory, camera start, etc.

b. Handshake -- Each time the HP calculator communicates with the TBC buffer, a signal is sent and returned that the instruction has been received and completed. Four handshake conditions are used:

- Command byte
- Write with each data word
- Read
- Read and EOF (end of frame-camera).

c. Timing -- Accurate simultaneous and sequential signals are generated in this section for internal buffer usage and to properly time peripheral activity. These timing signals affect addressing, chip select, write enable, DAC strobing, the A/O modulators, and the camera and video store. Reset restores all buffer registers to zero.

d. Multiplex -- The access time of the memory chips is long enough to be a problem at 50 MHz. The memory is therefore multiplexed, with this circuit controlling chip access to easily satisfy the speed requirement.

e. Peripherals -- These are the two A/O modulators, the 100 x 100 array camera, and the video memory. These devices are initialized, started, stopped, and reset by program control.

4. Address Generator -- The address generator is a 12 bit synchronous binary counter of which 10 bits are used to provide addresses A0-A9. These address lines take two paths. The first path is through line buffers directly to memory $A_1$ and memory $B_1$. The second path is to a 10 bit register which at a later time is accessed (during multiplexing), then through line buffers to memory $A_2$ and $B_2$.

5. Memory -- Memory A consists of sixteen 1024 word, 8 bit memory chips in two sections ($A_1$, $A_2$) of 8 chips each, as does memory B. Memory $A_1$ and $B_1$ are simultaneously addressed, chip selected, and write enabled; Memory $A_2$ and $B_2$ are simultaneously delay addressed, chip selected, and write enabled. The delay is the multiplex operation. Each section is alternately written (and alternately read) to the program-selected number of words. Writing the memories is done at HP 9825 DMA speed (200K words/sec). Reading has the same format as writing but the output data rate is 50 mega-words/sec.

6. Parity and Display -- As each input data word is processed, a parity bit is generated and placed in a small parity memory. When data is output, the parity checker compares the newly generated

parity value with the value in parity memory. If these are different, an error bit is counted and translated to an LED display.

7. Demultiplexer -- Data from the output ports of memory $A_1$ and $A_2$ are logically OR'd to provide a combined output data rate of twice the 25 MHz clock frequency. The same thing is done for memory $B_1$ and $B_2$. The results are sent to data line drivers.

8. Line Drivers -- The line drivers provide true and complimentary outputs which can be transmitted on twisted pair leads. Twisted pair transmission lines of several inches length can be used to supply these fast signals to the CACs which are mounted adjacent to the TBC buffer board.

9. DAC -- The ECL digital-to-analog converters are Tektronics DAC 850s. These are 8 bit converters capable of a 50 MHz update rate. The analog output is gain and offset adjustable.

### 4.2.2 RF Driver/Modulator (RFDM)

RFDM I drives Bragg cell I at a center frequency of 45 MHz. RFDM II drives Bragg cell II at a center frequency of 75 MHz. Both drivers were designed for suppressed carrier amplitude modulation. If we place a signal with a bandwidth of 0.25 Hz on a 0.4 Hz subcarrier, and choose a sampling rate of 5 poinds/ carrier cycle, the 50 MHz data rate from the TBC buffer will upshift the carrier frequency to 10 MHz and the bandwidth to 6.25 MHz.

### 4.2.3 Data Preparation

Initially, the NOSC synthetic data resided on a magnetic tape. This tape was read by a Honeywell Level6 minicomputer at CTC and its contents transferred to the Level6 disk storage, where it can easily be accessed for data preparation. A data preparation program has been written to place this data on a carrier frequency, add a bias to generate only positive 8 bit values from 0 to 255, combine an 8 bit data point from each signal into one 16 bit word, and store the prepared data in a disk file for transfer to the HP 9825A calculator.

The data transfer from the Level6 to the HP 9825 will occur through a special HP interface by way of a 300 baud telephone line. A transfer program has been conceived allowing the HP 9825 to decode the data and store it on its floppy disk system. Once the data is on the floppy disk system, it will be ready for multiple write operations to the TBC buffer.

## 4.3 REAR END ELECTRONICS

### 4.3.1 Two Dimensional Detector Array Camera

The detector array camera is a Reticon MC520 with a RS520 controller. The camera consists of 10,000 segmented photodiodes in a 100 x 100 matrix; it has a dynamic range of 200 to 1. The maximum pixel scan rate of 5 MHz translates into a frame rate of 500 frames/sec. The camera gives a positional signal for x and y and a video signal for z. It can, therefore, be used with a CRT with a z input terminal. The camera control signals are provided from the timing control circuit in the TBC buffer.

### 4.3.2 Video Memory

A video memory made by Applied Micro Technology will be used. It is designed to interface exclusively with the Reticon detector array camera, and can capture a single frame when the frame rate is 500 frames/sec. The value of each of the 10,000 photodiodes in the detector array will be digitized to 8 bits accuracy and stored. The stored frame can be continuously displayed on a refresh CRT. The digitized data can also be sent to the HP 9825A calculator for further analysis.

## SECTION 5
## SUMMARY

This project had two major objectives. The first objective was to demonstrate nonreal time generation of ambiguity functions from one dimensional input transducers. The second objective was to design front end and rear end electronics capable of supporting real time operation of the optical processor. Both of these objectives were successfully achieved, and in addition, a new optical architecture was invented (LIPS), and its feasibility and superiority was experimentally demonstrated.

The optical system demonstrating the proposed Passive Optical Tau-Shift concept (POTS) was designed with a large f number (>20) for aberration-free performance, and the system length became 12 meters. One dimensional Bragg cell-sized photographic transparencies were used to generate ambiguity functions. The results of processing both analytic V-FM signals and synthetic data from NOSC showed excellent agreement with theoretical predictions in terms of the correlation peak height and resolution.

Another optical architecture based on an entirely new concept of a space variant Linear Phase Shifter (LIPS) was independently developed. It generates a $\tau$-shift by a shear operation instead of the rotation used in POTS. Nonreal time experiments demonstrated good agreement with theory in terms of correlation peak height and resolution, and excellent, distortion-free output. The advantages of the LIPS approach are compactness, fewer optical components, and the elimination of the rotated coordinate systems which are in the POTS approach.

The real time system design can achieve a 50 MHz digital data rate in the front end electronics and a 500 frames/sec frame rate in the rear end electronics. The processing system will have a system TBW of 240, and any of the frames being generated at a 500 frames/sec rate can be captured, digitized, and stored for later evaluation either by a minicomputer or a large computer system.

## REFERENCES


1. L.J. Cutrona, E.N. Leith, C.J. Palermo, and L.J. Porcello, "Optical Data Processing and Filtering Systems", IRE Trans. IT-6, 386 (1960).

2. K.A.K. Said and D.C. Cooper, "Crosspath Real Time Optical Correlator and Ambiguity Function Processor", Proc. IEE 120, 423 (1973).

3. R.J. Marks II, J.F. Walkup, and T.F. Krile, "Ambiguity Function Display: an Improved Coherent Processor", Appl. Opt. 16, 746 (1977).

4. D. Casasent and B.V.K. Vijaya Kumar, "Optical Image Plane Correlator for Ambiguity Surface Computation", Appl. Opt. 18, 1673 (1979).

5. P.N. Tamura, J.J. Rebholz, and T.C. Lee, "Ambiguity Map Generation with Coherent Optics", J. Opt. Soc. Am. 69, 1451 (1979).

6. A. Rihaczek, Principles of High Resolution Radar (McGraw-Hill, Hill, New York, 1969).

7. C.E. Cook, M. Bernfeld, Radar Signals (Academic Press, New York, 1967).

END

DATE
FILMED

8-80

DTIC